

Organic–inorganic hybrid liquid crystals derived from octameric silsesquioxanes. Effect of the peripheral groups in mesogens on the formation of liquid crystals

Xiaobai Wang,^a Ching Mui Cho,^a Wan Yong Say,^{ab} Angeline Yan Xuan Tan,^a Chaobin He,^{ac} Hardy Sze On Chan^b and Jianwei Xu^{*a}

Received 9th October 2010, Accepted 5th January 2011

DOI: 10.1039/c0jm03406a

A series of octameric silsesquioxane-based organic–inorganic hybrid compounds **7a–h** was synthesised by reacting octakis(dimethylsiloxy)silsesquioxane with 4'-(undec-10-enyloxy)biphenyl-4-yl mono-, di-, or trialkoxybenzoate *via* platinum-catalysed hydrosilylation reaction. The chemical structures of **7a–h** were characterised by ¹H, ¹³C, and ²⁹Si nuclear magnetic resonance spectroscopy, mass spectroscopy and elemental analysis. Liquid crystallinity of **7a–h** was investigated by differential scanning calorimetry (DSC) and polarised optical microscopy (POM). Temperature-dependent X-ray diffraction was used to verify liquid crystal phases, revealing that **7a–d** assembled to smectic C and smectic A phases. The effects of the number and length of peripheral flexible alkoxy groups in **7a–h** on the formation of liquid crystals were studied using DSC and POM, which revealed that **7a–d** bore one alkoxy terminal group in each mesogen exhibited a mesophase, **7e–f** and **7g–h** bore two and three flexible alkoxy terminal groups in each mesogen, respectively, and did not show mesomorphic behaviour. The concept of “flexible group density” (FGD), which was defined as the number of the CH₂ groups per unit volume in the periphery of the POSS molecule, was introduced to interpret the formation of liquid crystals. The results revealed that the POSS molecules with di- and tri-substituted mesogens exhibited much larger FGD than those with mono-substituted mesogens, hence the absence of mesophases for **7e–f** and **7g–h**. This study provides a useful archetype to predict the formation of liquid crystals when designing and synthesising liquid crystalline materials, particularly star-like or dendrimer-like molecular materials.

Introduction

Among the useful candidates for forming inorganic–organic hybrid materials, polyhedral oligosilsesquioxanes (POSS), particularly the cube-like octameric silsesquioxanes [(SiO_{3/2})₈R₈], have attracted much interest during the past two decades.^{1,2} Octameric silsesquioxane has a stable, compact chemical structure and can be regarded as an inorganic nano-particle with Si–O–Si bonds and Si corners. This stable cubic structure can be modified by adding different types of organic functional groups to the Si corners *via* suitable chemical reactions, and thus a variety of hybrid materials can be achieved.^{3–15} Due to the unique characteristics of POSS, it has been used as a core to develop organic–inorganic hybrid liquid crystalline materials. The first octameric silsesquioxane-containing liquid crystal (LC)

was reported in 1991,¹⁶ after which a number of POSS-based LCs were generated by introducing different mesogens in the corner chains.^{17–23} These POSS-based LCs are generally prepared starting from the octameric silsesquioxanes such as (Si₈O₁₂)H₈ or (Si₈O₁₂)(OSi(Me)₂H)₈, which allow for modification with a variety of mesogens *via* hydrosilylation in the presence of a suitable platinum catalyst. The sizes and structures of these LC materials could be well controlled by attaching different mesogens, revealing that various mesophases could be formed by governing the shape of the mesogens, the spacer length between the mesogen and the POSS core as well as the number of substituted corner chains. For instance, the inclusion of lateral attachments of calamitic mesogens, incomplete substitution of the POSS core, or involvement of nematogenic mesogens in the POSS side corner chains can lead to the formation of nematic phases.^{16,22–25} By introducing chiral nematic mesogens to the silsesquioxane core with a moderate spacer length to control the strength of coupling (interaction) between the POSS core and mesogens, only the chiral nematic phase could be observed. However, mesogens, such as 4'-ω-alkynyl-4-cyanobiphenyls²⁶ and bent-core mesogens,^{22,27} that are attached to the POSS core led to the formation of a thermotropic smectic phase, a smectic CP or

^aInstitute of Materials Research and Engineering, 3 Research Link, Singapore, 117602. E-mail: jw-xu@imre.a-star.edu.sg; Fax: +65-6872-7528; Tel: +65-6872-7543

^bDepartment of Chemistry, National University of Singapore, Singapore, 3Science Drive 3, 117543

^cDepartment of Materials Science & Engineering, National University of Singapore, 5 Engineering Drive 2, Singapore, 117576

a nematic phase. Columnar assemblies, such as rectangular and hexagonal columnar mesophases, could be observed for lateral mesogen-modified POSS-based LCs. Furthermore, the strength of the coupling between the POSS core and mesogens could be adjusted by changing the spacer length between the mesogens and the POSS core and subsequently controlling the POSS-based LC supramolecular assembly.²⁸ When the spacer length between the mesogens and the POSS core is short, for example, two CH₂ units, a “column-within-column” hexagonal columnar phase is formed. In contrast, when the spacer length increases to six or ten CH₂ units, it tends to form rectangular or hexagonal columnar phases.

Flexible chains are usually linked to various mesogens, and their functions are mostly to modulate the thermal properties, solubility, processability and assembly architectures. However, studies on the effect of peripheral flexible chains on the formation of LCs are scarce. Peripheral flexible chains attached to the mesogen are of the utmost importance in adjusting the thermal properties, particularly phase transition temperatures, of LCs. The number, size (length) and even shape of the flexible chains will have an effect on the thermal properties, morphology and assembly of LCs. Therefore, proper selection of flexible chains in suitable numbers would be valuable in forecasting the possibility of LC formation as well as the assembly structures. In this paper, we report on the synthesis, structure and LC properties of a series of octakis[(11-(4'-(1-(4-alkoxy,3,5-dialkoxy or 3,4,5-trialkoxybenzoyloxy)biphenyl-4-yloxy)undecyl)dimethylsiloxy)]silsesquioxanes. The spacer length between the POSS core and mesogens is fixed to be -(CH₂)₁₁Si(Me)₂O-, which is approximately equivalent to the length of thirteen methylene units, thus minimising the coupling between the POSS core and mesogens. Mesogens with one, two or three terminal alkoxy groups are

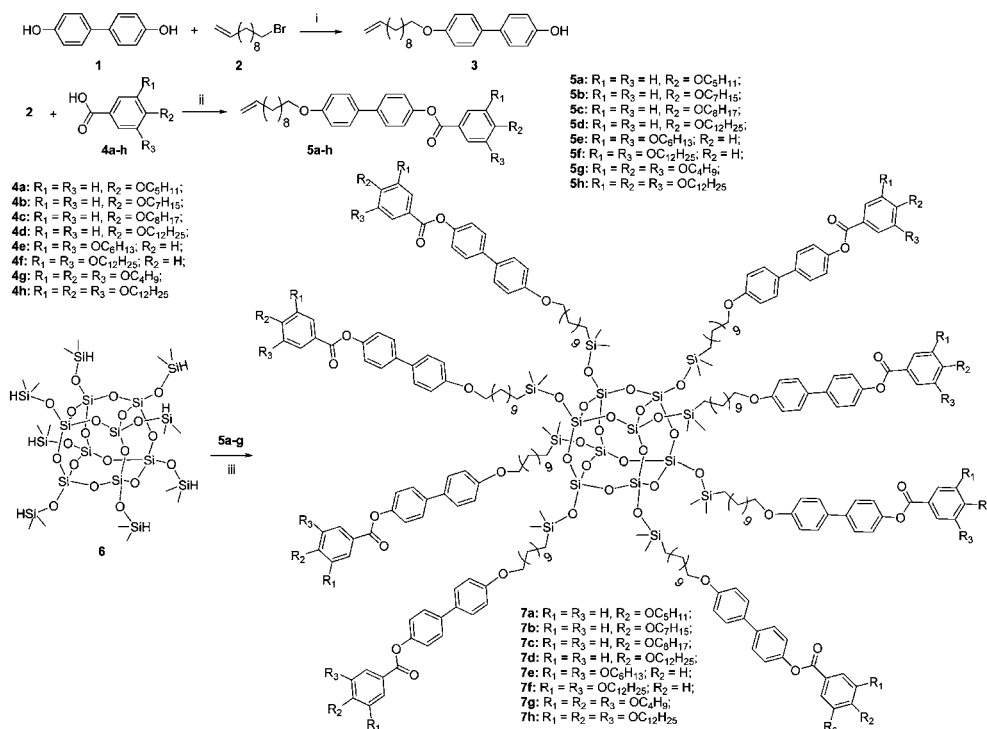
selected to attach to the POSS core *via* a platinum-catalysed hydrosilylation reaction. The effect of the length and number of peripheral alkoxy groups in each mesogen on the formation of LCs is explored. The phase transitions, thermal properties, and corresponding structural changes are studied using differential scanning calorimetry (DSC), polarised optical microscopy (POM) and variable temperature X-ray diffraction (XRD). The study reveals that the formation of LCs is controlled by varying the length and the number of the terminal alkoxy groups in the mesogens. When the mono alkoxy terminal group is attached to each mesogen, the POSS derivatives exhibit the smectic phases. However, when two or three alkoxy terminal groups are attached in each mesogen, no mesophases are formed.

Results and discussion

Synthesis and structural characterisation

The synthetic routes leading to compounds **7a–h** are shown in Scheme 1. Alkenyl precursor compounds **5a–h** were prepared by reacting excess biphenyl-4,4'-diol (**1**) with 11-bromoundec-1-ene (**2**) in the presence of anhydrous K₂CO₃ in DMF, followed by esterification using *N,N'*-dicyclohexylcarbodiimide (DCC) and a catalytic amount of 4-dimethylaminopyridine (DMAP) according to a similar method previously reported, with modifications.²⁹

A hydrosilylation reaction between octakis(hydrodimethylsiloxy) octasilsesquioxane (**1**) with compounds **5a–h** was performed in dry toluene at room temperature with the catalyst platinum divinyltetramethyldisiloxane complex (Pt(dvs)) (Scheme 1).³⁰ An excess of **5a–h** was used to ensure that the hydrosilylation was complete. Crude products were purified by silica gel



Scheme 1 Synthesis route leading to compounds **7a–h**. Reaction conditions: i) K₂CO₃, dry DMF, 80 °C, 48 h; ii) DCC, DMAP, dry CH₂Cl₂, reflux for 16 h in argon. iii) Pt(dvs), dry toluene, 40 °C, overnight, N₂.

column chromatography to afford pure **7a–h**. All intermediates **5a–h** and final compounds **7a–h** were characterised by ^1H , ^{13}C , ^{29}Si NMR spectroscopy, and elemental analysis. The disappearance of the Si–H absorption at 2142 cm^{-1} in FT-IR spectra and the signal at 4.7 ppm in ^1H NMR spectra, in combination with ^{13}C and ^{29}Si NMR spectra, confirms exactly eight corner-substitutions. As an example, ^1H NMR and ^{29}Si NMR spectra of **7f** are given in Fig. 1 and 2, respectively. Two pairs of doublets at δ 7.57, 7.49, 7.23 and 6.95 were assigned to aromatic protons with AB splitting systems (biphenyl part). Two singlets at δ 7.32 and 7.71 correspond to 3,5-disubstituted phenoxy protons. The proton integration ratio of $-\text{OSi}(\text{CH}_3)_2-$ at δ 0.15 and $-\text{OCH}_2-$ at δ 4.00 was 1 : 1, which is the same as the theoretical value, confirming the formation of octa-substitution in the detection limit. In the ^{29}Si NMR spectrum of **7f**, two singlets at δ 12.75 and -108.65 , which are assigned to the Si atom on the side chains and the cage Si atom, respectively, were observed, indicating the octameric cage structure is intact during the synthesis. A pseudo-triplet at δ 0.6 and the absence of signals at δ 2.5 both indicate that the addition of the Si–H bond to the alkene **5a–h** ($\text{CH}_2^{\beta}=\text{CH}^{\alpha}-\text{R}$) affords regiospecific β -addition products, consistent with reported examples.³¹ **7a–h** are white solids or low melting point waxy solids at room temperature and are soluble in common organic solvents such as tetrahydrofuran, chloroform, *etc.*

Thermal behaviour and textures studied by DSC and POM

The thermal behaviours of molecules **7a–h** were examined using DSC. Their corresponding phase transition temperatures and

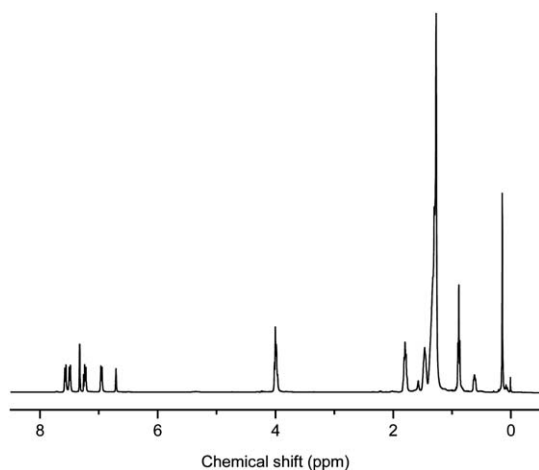


Fig. 1 ^1H NMR spectrum of **7f** in CDCl_3 at room temperature.

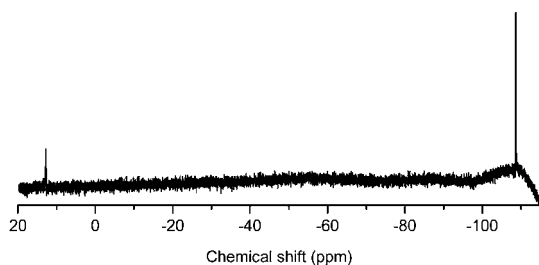


Fig. 2 ^{29}Si NMR spectrum of **7f** in CDCl_3 at room temperature.

Table 1 Thermal behavior of **7a–h**^a

POSS	Transition $T/^\circ\text{C}$ (Enthalpy/ kJ mol^{-1})	
	Heating	Cooling
7a	Cr 124(53.7) S 220(37.5) I	I 213(42.9) S 115(50.1) Cr
7b	Cr 122(181.3) S 233(98.8) I	I 227(81.2) S 106(148.1) Cr
7c	Cr 127(213.3) S 232(106.4) I	I 227(95.9) S 112(186.1) Cr
7d	Cr 119(47.5) S 211(39.8) I	I 199(41.8) S 111(52.6) Cr
7e	Cr $-8.5(13.1)$ I	I $-14.0(17.1)$ Cr
7f	Cr $-0.9(13.2)$ I	I $-4.0(16.4)$ Cr
7g	Cr 39.7(68.2) I	I $-14.5(26.1)$ Cr
7h	Cr 25(108.9) I	I 10(71.5) Cr

^a Cr, crystalline; S, smectic phase; I, isotropic phase. Transition temperatures ($^\circ\text{C}$) were taken from second run of the DSC thermo diagram.

associated enthalpy changes of transition are also summarised in Table 1. Compounds **7a–d** that have only one flexible alkoxy terminal group in each mesogen displayed multiple phase transitions on heating and on cooling, indicating the formation of mesophase. As examples, the DSC thermograms of compounds **7b** and **7c** are shown in Fig. 3. In Fig. 3a, it is clearly shown that both **7c** and **7d** displayed mesophases upon heating and cooling. At first glance, only two major phase transitions in the DSC thermogram of **7c** are observed on heating and on cooling. However, a few small endothermic peaks with much lower enthalpy changes from 0.21 to 1.17 kJ mol^{-1} than that of the major transition, which occurred at $232\text{ }^\circ\text{C}$ (106.4 kJ mol^{-1}), are observed in an enlarged DSC thermogram of **7c** between $120\text{ }^\circ\text{C}$ and $210\text{ }^\circ\text{C}$ on the second heating (Fig. 3b). Similarly, a few small corresponding exothermic peaks are also found on the second cooling. Besides **7c**, other liquid crystalline compounds, such as **7a–b** and **7d**, show analogous transition behaviour, although these transitions are not as obvious as those for **7c**. These negligible phase transitions of **7c** have been detected by POM, and they roughly correspond to texture changes, as shown in Fig. 4. The texture changes observed at 134, 145, 168, 187 and $197\text{ }^\circ\text{C}$ correspond to the phase transitions observed in the DSC curve at 130, 146, 165, 182 and $197\text{ }^\circ\text{C}$, respectively. The enthalpy change for negligible transitions is around 1% compared to the enthalpy changes of major transitions. A few unusual textures, particularly, shown in Fig. 4a and b are observed, which are assigned to unidentified LC phases. Fig. 4c–f display a broken fan-shaped texture, a typical smectic C (SmC) phase. In contrast, a focal conic fan texture was observed in Fig. 4h, which is a characteristic texture of a smectic A (SmA) phase (see below). Therefore, the transitions with very small enthalpy changes mostly correspond to the textures of LC phases although it is hard to completely rule out that some of these subtle enthalpy changes are due to the intramolecular molecular movement of the POSS corner chains.

As shown in Table 1, **7a–h** show larger enthalpy changes than conventional LCs. Similar observations with large enthalpy changes have been found in other POSS-based LCs.²⁸ This is likely due to the eight bulk mesogenic groups surrounding the POSS core, which may enhance the intra-molecular interactions. The identification of mesophase was studied by POM, revealing that **7a–d** exhibit SmC phases at relatively lower temperatures and SmA phases at relatively higher temperatures. As an example, polarised optical photographs of **7c** and **7d** during

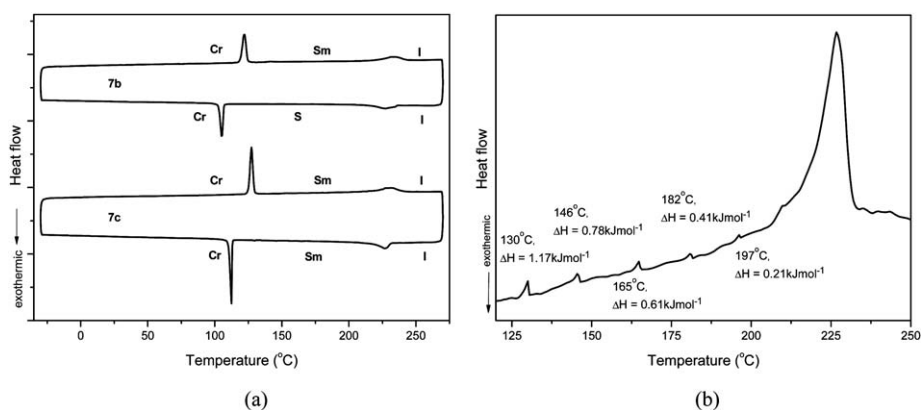


Fig. 3 a) DSC thermograms of **7b** and **7c**, the 2nd run. b) Enlarged part of DSC diagram of **7c** from 120 °C to 250 °C on heating. Small enthalpy changes between 125–200 °C show different phase transitions.

cooling are shown in Fig. 5. **7c** and **7d** exhibited typical focal conic fans, corresponding to SmA phases. At the lower temperature, they displayed broken fan textures, revealing the formation of SmC phases. It is worth noting that a less ordered nematic phase was not observed for **7a–d**. The octa-substitution increases the local concentration of the mesogens upon attachment to the POSS core, suppresses the formation of less-ordered nematic phases and thus leads to higher-ordered phases.³² Compounds **7e–f** and **7g–h** have two and three flexible terminal groups in each mesogen, respectively, but they did not exhibit mesomorphic behaviour, as evidenced by the absence of mesophase transitions in their DSC thermograms, which is verified by POM as well.

For POSS compounds **7a–d** with mono-alkoxy substituted mesogens, the alkoxy chain lengths from OC₅H₁₁ to OC₁₂H₂₅ in the mesogenic side chains have a certain impact on changes in the phase transition temperatures (Table 1), but there is no fixed correlation between the phase transition temperatures and lengths of the alkoxy chain. For example, on the second heating, the crystalline–smectic transition temperatures (T_{Cr-S}) increased from 213 to 227 °C for OC₅H₁₂ and OC₈H₁₇, respectively, and then slightly decreased to 119 °C for OC₁₂H₂₅. Likewise, smectic–isotropic transition temperatures (T_{S-I}) followed the

same trend as the T_{Cr-S} . On the second cooling process, the isotropic–smectic transition temperatures (T_{I-S}) and smectic–crystalline transition temperatures (T_{S-Cr}) exhibited the same trend as the T_{Cr-S} and T_{S-I} during the heating process. This could be because the increase in alkoxy chain lengths (by a few methylene units) is much less significant in contrast to the large volume of the whole POSS molecule. As a result, there are no significant variations for transition temperatures.

In contrast, more substitution with long alkoxy chains in mesogens has a significant effect on the thermal behaviour of the POSS-based molecules, and it will lead the mesophase to disappear due to the depression of the order of the LC orientation. Additional long flexible alkoxy chains in the mesogens will impose extra freedom on the motion of these flexible terminal chains and, thus, significantly reduce the phase transition temperatures. For instance, the melting temperature of **7h** is about 200 °C lower than that of T_{S-I} of **7a–d**. Similar observations have been reported in some star-like hydrogen-bonded LCs.³³ When one alkoxy chain is attached to the periphery of mesogens, hydrogen bonded complexes form LCs. However, when two or three long alkoxy chains (OC₁₂H₂₅) are attached to the periphery of mesogens, hydrogen bonded LCs disappear.

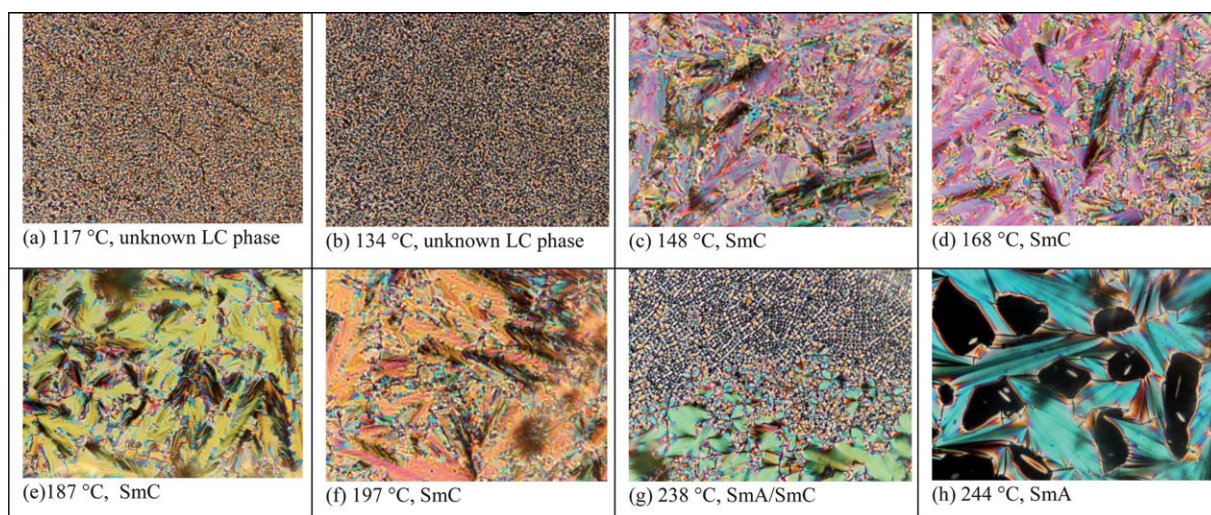


Fig. 4 Texture changes of **7c** in the temperature range of 244 to 117 °C on heating. All the textures observed by POM correspond to the phase transitions in the DSC diagram.

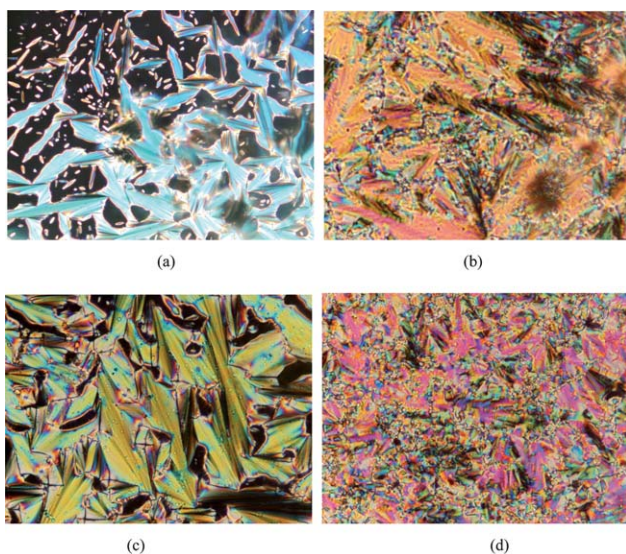


Fig. 5 Polarized optical photograph of (a) **7c** at 244 °C on cooling; (b) **7c** at 200 °C on cooling; (c) **7d** at 213 °C, on cooling; (d) **7d** at 175 °C, on cooling.

Substituted POSS is considered to be a spherical molecule with a volume estimation based on the length of the corner substituents and size of the inorganic core, using the Chem 3D Pro program. We introduced the term “flexible group density” (FGD), which is capable of estimating how many flexible units per unit volume are in the periphery of the POSS molecule and thus can act as an indicator to determine/predict the formation of LCs. The FGD in the periphery of the POSS molecules is defined as the ratio of the total number of carbon atoms in the flexible chains to the periphery volume that flexible chains occupy, which is calculated by subtracting the volume of the central core, consisting of the POSS inorganic core, spacer and mesogenic part, from the whole POSS molecule. The FGD is calculated in terms of the following equation, where R and r represent the radii of the whole POSS molecule and the central core consisting of the POSS inorganic core, spacer and mesogenic parts, respectively.

Flexible group density in the periphery

$$= \frac{8 \times \text{no. of carbon atoms in the alkoxy groups}}{\frac{4}{3}\pi(R^3 - r^3)}$$

As mentioned above, the POSS can be regarded as a spherical molecule, so the value of r is equal to the sum of the radius of the POSS inorganic core, the length of spacer and the length of mesogen; whereas, the value of R is equal to the sum of r and the length of the flexible chain.¹⁹ Based on the above definition, the overall volume of a POSS molecule with mesogens substituted by a single flexible group is approximately close to that of a POSS molecule with mesogens substituted by two or three identical flexible groups. Therefore, an increase in the number of flexible groups on the mesogens will lead to an increase in FGD (Table 2). The calculated FGD values for **7a–d** ranging from 3.16×10^{-4} to $2.65 \times 10^{-4}/\text{\AA}^3$ are much smaller than those of **7e–f** (16.5×10^{-4} and $9.30 \times 10^{-4}/\text{\AA}^3$, respectively) and **7g–h** (15.3×10^{-4} and $11.3 \times 10^{-4}/\text{\AA}^3$, respectively), suggesting that additional long flexible substitutions on **7e–h** result in excess flexibility to the

Table 2 Flexible group density (FGD) in the periphery of **7a–h**

POSS	FGD ($\times 10^4/\text{\AA}^3$)	POSS	FGD ($\times 10^4/\text{\AA}^3$)
7a	3.16	7e	16.5
7b	3.05	7f	9.30
7c	2.92	7g	15.3
7d	2.65	7h	11.3

whole POSS molecule and produce a more disordered packing structure than **7a–d**. Therefore, **7e–h** behave more liquid-like and do not exhibit any mesomorphic behaviour (Fig. 6).

Incorporation of a few flexible groups into a mesogen is a common method to make a liquid crystal. Multiple substitution with flexible groups in the peripheral mesogens results in the formation of columnar or other liquid crystalline structures in a variety of self-assemblies. For discotic-like or planar molecular LCs, either the mesogen itself acts as the central core, or mesogens directly link to a planar central core³⁴ through covalent linkages, *e.g.*, an ester linkage, to develop LC states as illustrated in Fig. 7a. Development of LC state, however, usually occurs when there is no flexible spacer between the mesogens and the planar central core, and multiple (di- or tri-) substitution in the mesogens will not lead to loss of LCs. In contrast, liquid crystalline spherical molecules derived from a three-dimensional core, such as a cyclotriphosphazene ring or POSS core, could be simply categorised into two typical models in which they contain

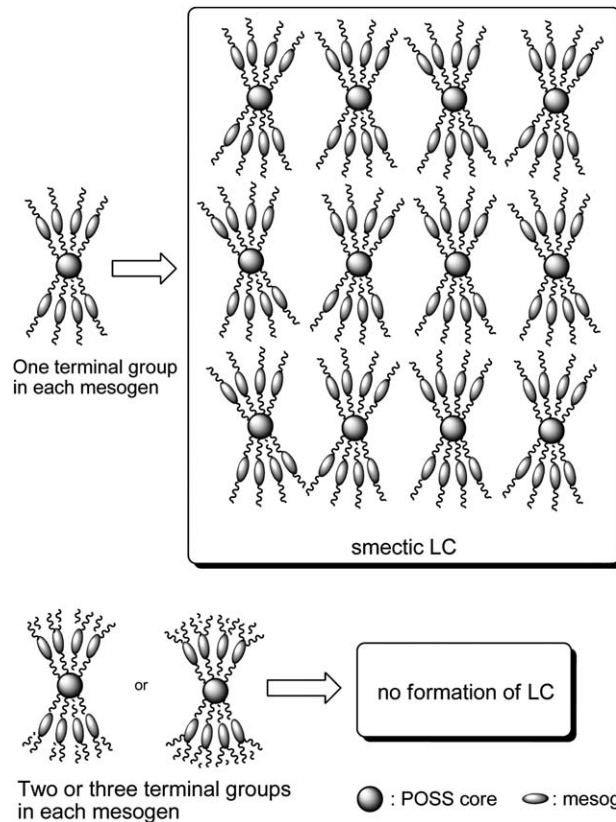


Fig. 6 The effect of peripheral flexible groups in mesogens on the formation of liquid crystals.

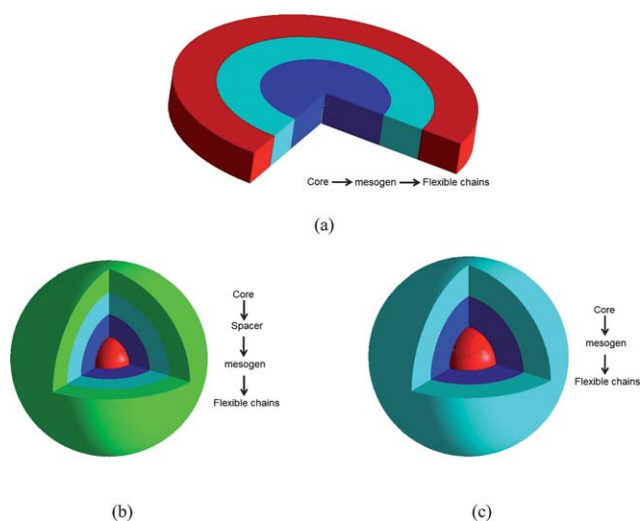


Fig. 7 The schematic representations of three types of LCs derived from a planar molecule (a), a three-dimensional core with (b) or without a spacer between the internal core and mesogens (c).

or do not contain spacers between the three-dimensional central core and mesogens, as shown in Fig. 7b and c, respectively. If there is no spacer, it will result in a strong coupling between the central core and mesogens. Similar to the molecule with a planar core, multiple substitution in this model causes changes only in the architecture of molecular assembly and, thus, gives rise to different mesomorphisms instead of the disappearance of LC. For example, cyclotriphosphazene,³⁵ in which each mesogen contains only one flexible chain, yields a nematic phase. In contrast, mesogenic moieties that consist of two or three long flexible chains exhibit columnar mesophases. In this study, the spacer length between the POSS core and mesogens is equivalent to thirteen CH₂ units, which is long enough to make the POSS core and mesogens decouple. Thus, the formation of LC will largely rely on the relative magnitude of FGD in the periphery, multiple substitutions will lead to more flexible units surrounding the periphery of the molecule, and, hence, the molecule is more likely to behave as a liquid. This liquid-like behaviour, in fact, could be evidenced by the dramatic drop in the melting temperatures of **7e** (−8.5 °C) and **7g** (39.7 °C) compared with that of **7d** (T_{C-S} : 119 °C and T_{S-I} : 211 °C), which has the same molecular weight as **7e** and **7g**.

Based on the above discussion, we can conclude that the number and length of peripheral groups are important factors not only to control the phase transition parameters and architectures of assembly, but also to determine the formation of mesophase. Therefore, it would be essential to select the suitable number and length of peripheral flexible groups when designing and synthesising star-like and dendrimer-like liquid crystalline materials.

X-Ray diffraction study of POSS-based LCs

Variable-temperature wide angle XRD was performed to verify the liquid crystal phases observed. Using **7c** as an example, the X-ray diffraction data of **7c** on heating are summarised in Table 3. Fig. 8 shows the variable-temperature wide angle X-ray diffraction (WAXD) of compound **7c**. At room temperature, it is crystalline and shows multiple diffraction peaks at 4.75, 7.09,

8.05, 13.20, 19.59, 22.0 and 27.48°. A strong scattering at a low angle of 4.75° (2θ) indicates the presence of a lamellar structure. When it was heated up from room temperature to 120 °C, a strong, sharp scattering at 4.71° (2θ) remained, accompanied by two strong diffraction peaks at 19.4° (2θ) and 7.0° (2θ). The strong liquid-like broad scattering at 7.0° (2θ), corresponding to the d -spacing of 12.7 Å, is due to the Si–O clusters in the POSS core.^{16,19,21,36,37} Similar observations have been reported in some siloxane-based liquid crystalline polymers and in some siloxane core-based LCs.³⁸ The first order diffraction is too weak to be observed within the angular range of the XRD experiment. The strong scattering at 4.71° corresponds to a d -spacing of 18.8 Å, indicating a second-order diffraction peak. The volume of **7c** is estimated to be 43 Å by the Chem 3D Pro program. As the measured d -spacing of the second-order diffraction is 19 Å, the corresponding d -spacing for the first-order diffraction should be equal to 38 Å, which is shorter than the modelled estimation, indicating the presence of the interdigitated structure involving the overlapping of the flexible chains between neighbouring layers.

To exactly identify the phase transitions, XRD graphs from 200 to 250 °C with the calculated d -spacings of the second-order diffractions are shown in Fig. 9. When the measuring temperature increases from 200 to 240 °C, the d -spacing of the second-order diffraction remains unchanged. When temperature increases from 240 to 250 °C, the d -spacing of the second-order diffraction increases from 18.4 to 19.0 Å. This gives strong evidence for the formation of the tilted SmC phase. In contrast to a SmA phase, in which the director is perpendicular to the smectic plane, POSS molecules in a SmC phase assemble to an arrangement approximately parallel to layers in which the director is tilted with respect to the normal layer. In terms of d -spacing of the second-order diffraction, the tilt angle is estimated to be 15°. In fact, the change in the d -spacing of the second-order diffractions at the low angle is in good agreement with the texture changes observed by POM, which reveal the characteristic broken fan of a SmC phase at 200 °C and conic fan texture of a SmA phase at 244 °C (Fig. 4).

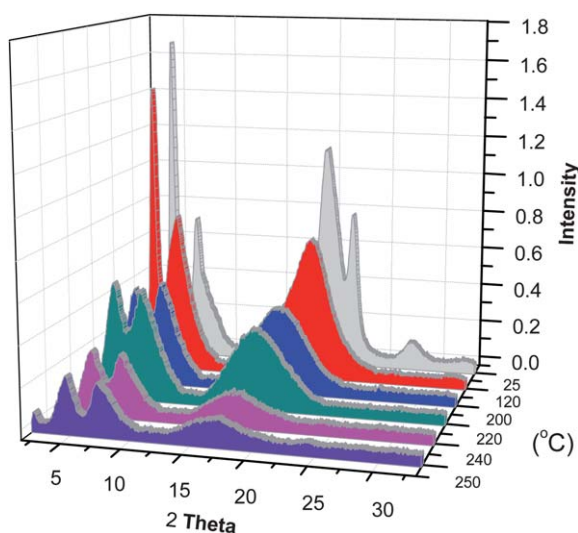
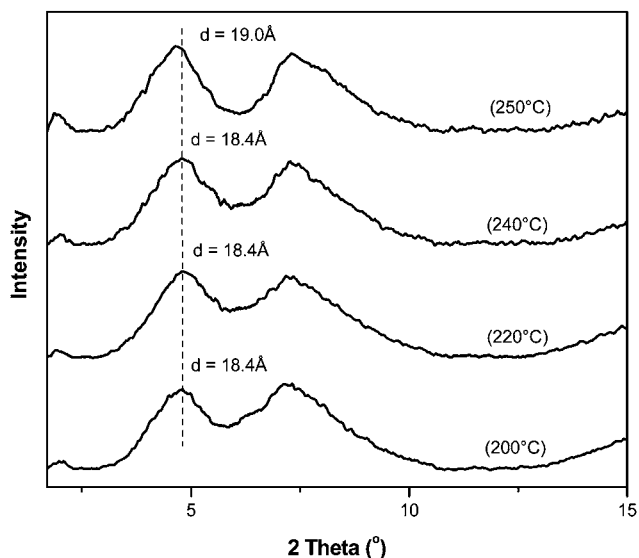
Conclusions

In summary, we synthesised a series of organic–inorganic hybrid POSS-based LCs. The chemical structures of **7a–h** were characterised by ¹H, ¹³C, and ²⁹Si NMR, mass spectroscopy and elemental analysis. Temperature-dependent X-ray diffraction was used to verify mesophases, revealing that **7a–d** showed SmC and SmA phases. The DSC also showed that minor exothermic and endothermic transitions with very small enthalpy changes were detected. These subtle transitions corresponded to the texture changes observed by POM. Three molecular models and the FGD concept were proposed to address the effect of the flexible chain on the formation of LCs. The number and length of the FGD in the periphery surrounding the mesogenic and POSS core have a significant effect on determining the formation of LCs, particularly when the coupling between the central core and mesogens is minimised. The POSS-based LCs with mesogens substituted by single flexible chains tended to form smectic mesophases. When the mesogens were substituted by two or three flexible chains, LCs disappeared. These observations strongly supported the hypothesis that the FGD in the periphery

Table 3 X-ray diffraction data of **7c** at different temperatures on heating^b

<i>T</i> /°C	2θ/ <i>d</i> -spacings	
	diffractions (2θ)	<i>d</i> -spacing (Å)
25	4.75, 7.09, 8.05, ^a 13.20, 19.59, 22.0, 27.48	18.59, 12.46, 10.98, 6.70, 4.53, 4.04, 3.24
120	4.71, 6.96, 19.42	18.75, 12.69, 4.57
140	4.69, 6.87, 19.17	18.83, 12.86, 4.63
160	4.63, 6.86, 18.86	19.07, 12.88, 4.70
180	4.53, 7.07, 18.54	19.50, 12.50, 4.78
200	4.79, 7.22, 17.89	18.44, 12.24, 4.96
220	4.79, 7.27, 17.27	18.44, 12.15, 5.13
240	4.79, 7.36, 17.05	18.44, 12.00, 5.20
250	4.66, 7.33, 17.00	18.96, 12.06, 5.22

^a Shoulder peak. ^b Very weak peak.

**Fig. 8** X-ray diffraction patterns from 25 to 250 °C.**Fig. 9** X-ray diffraction patterns at the low angle region at the temperature from 200 to 250 °C.

of the POSS-based star-like molecules is a key feature for determining the formation of LCs. This study could offer a useful and pragmatic guideline to predict the formation of LCs when designing and synthesising star-like, or even dendrimer-like, liquid crystalline materials. Further studies focusing on how the coupling between a POSS core with reduced spacer length and mesogens, as well as the peripheral flexible groups, jointly and interdependently affects the formation of LCs are currently under way in our group.

Experimental section

Instrumentation

The ¹H, ¹³C and ²⁹Si NMR spectra were acquired on a Bruker DCR 400 MHz spectrometer in deuterated chloroform with tetramethylsilane as an internal standard. The operating frequency for ¹H, ¹³C and ²⁹Si are 400.1, 100.6 and 79.5 MHz, respectively. The coupling constant is expressed as “*J*” with units of Hz. Fourier transform infrared (FTIR) spectra were recorded on a Perkin-Elmer Fourier transform infrared spectrophotometer 2000 using KBr pellets. Thermal behaviors of compounds were studied on a TA instrument DSC 2920 under a heating and cooling rate of 5 °C min⁻¹ in nitrogen. The peak temperatures of the endo-thermo and exo-thermo were taken as the phase transition temperatures. The photomicrographs of the complexes were taken under a Nikon OPTIPHOT2-POL polarizing optical microscope fitted with a hot stage using a temperature programmer TP_93 and a TMC-6RGB1/2' color CCD camera. The sample was placed on a glass slide, cover with a glass cover slip and heated on the hot stage at 10 °C min⁻¹ and cooled at 2 °C min⁻¹. X-ray diffraction pattern was recorded on a Bruker GADDS X-ray diffractometer equipped with an external heating element using Kα radiation wavelength (λ = 1.5418 Å). The tube voltage and amperage were set to 40 kV and 30 mA, respectively, and 2θ step scans of 0.02° and a counting time of 0.2 s per step were used for all XRD measurements. The powdered samples were packed into very thin-walled capillary tubes, heated to their melt state and air-cooled to the room temperature before the X-ray diffraction patterns were recorded. Electron ionization mass (EIMS) spectra were recorded on a Micromass 7034E mass spectrometer. Elemental analysis was conducted on a Perkin-Elmer 240C elemental analyzer for C, H, and N determination.

Materials

Octakis(dimethylsiloxy)silsesquioxane (**6**) was purchased from Hybrid Plastics and dried in an oven at 40 °C overnight prior to use. 11-Bromo-1-undecene (**2**) was purchased from Alfa Aesar. *N,N*-Dicyclohexylcarbodiimide and 4,4'-dihydroxybiphenyl and other chemicals were bought from Sigma-Aldrich and used as received. Monoalkoxy, dialkoxy or trialkoxybenzoic acids were prepared according to reported methods.³³

Synthesis of compounds

4'-(Undec-10-enyloxy)biphenyl-4-ol (4). 11-Bromo-1-undecene (1.18 mL, 5.38 mmol), 4,4'-biphenol (5.00 g, 26.85 mmol) and potassium carbonate (3.71 g, 26.85 mmol) were added into dry *N,N*-dimethylformamide (DMF) (100 mL). The reaction mixture

was stirred at 80 °C for 48 h and then solvent was removed under reduced pressure. Dichloromethane was added into the solid residue. The suspension was stirred at room temperature for 15 min and then was filtered off. The dichloromethane was removed and the residue was recrystallized in dichloromethane to afford white solid **3**. Yield: 0.76 g, 42%.

¹H NMR δ [ppm]: 7.43(t, overlapped dd, 4H, Ar-H), 6.94 (d, 2H, $J = 8.4$ Hz, Ar-H), 6.88 (d, 2H, $J = 8.4$ Hz, Ar-H), 5.82 (m, 1H, HC=CH₂), 5.02 (m, 2H, HC=CH₂), 4.79(s, 1H, OH), 3.98(t, 2H, $J = 6.4$ Hz, OCH₂), 2.05(m, 2H, CH₂HC=CH₂), 1.79 (m, 2H, OCH₂CH₂), 1.51–1.25 (br, 12H, (CH₂)₆). ¹³C NMR δ [ppm]: 158.60, 154.86, 139.47, 134.11, 133.52, 128.19, 127.93, 115.85, 115.09, 114.37. Anal. Calc for C₂₃H₃₀O₂: C 81.62%, H 8.93%, found: C 81.35%, H 8.69%.

General synthetic procedures of 5a–h

4-n-Alkoxybenzoic acid (0.71 mmol), 4'-hydroxybiphenyl undecene-1-yl ether (0.20 g, 0.59 mmol) and dimethylaminopyridine (DMAP) (0.030 g, 0.24 mmol) were dissolved in 13.0 mL of dry dichloromethane. The reaction mixture was purged with argon gas for 10 min before the addition of dicyclohexylcarbodiimide (DCC) (0.19 g, 0.89 mmol) in 4.0 mL dry dichloromethane. The mixture was then refluxed for 16 h under argon gas protection. After the reaction is complete, the resulting suspension was removed by filtration. The filtrate was washed with water and dried, and the organic solvent was removed. The residue was column chromatographed on silica gel using a mixture of dichloromethane and hexane (V : V = 65 : 35) as eluent to afford **5** as a white solid.

4'-(Undec-10-enyloxy)biphenyl-4-yl 4-(pentyloxy)benzoate (5a). Yield: 73%. ¹H NMR δ [ppm]: 8.09 (d, 2H, $J = 8.8$ Hz, Ar-H), 7.50 (d, 2H, $J = 8.8$ Hz, Ar-H), 7.44 (d, 2H, $J = 8.4$ Hz, Ar-H), 7.17 (d, 2H, $J = 8.4$, Ar-H), 6.90 (dd, 4H, $J = 8.8$ Hz, Ar-H), 5.76 (m, 1H, HC=CH₂), 4.90 (m, 2H, HC=CH₂), 3.98 (t, 2H, $J = 6.6$ Hz OCH₂), 3.93 (t, 2H, $J = 6.6$ OCH₂) 1.98 (m, 2H, CH₂HC=CH₂), 1.74 (m, 4H, OCH₂CH₂), 1.40 (m, 4H, OCH₂CH₂CH₂), 1.38–1.19 (m, 12H, (CH₂)₆), 0.88(t, 3H, $J = 6.8$, CH₃). ¹³C NMR δ [ppm]: 165.45, 163.94, 159.17, 150.43, 139.56, 138.93, 133.24, 132.65, 128.45, 128.02, 122.33, 122.04, 115.24, 114.70, 114.47, 68.72, 68.53, 34.15, 29.87, 29.78, 29.74, 29.68, 29.48, 29.30, 29.17, 28.51, 26.42, 22.78, 14.32. EI-MS (m/z): Found: 528.4. Calc.: 528.7. Anal. Calc for C₃₅H₄₄O₄: C 79.51%, H 8.39%, found: C 79.05%, H 8.16%.

4'-(Undec-10-enyloxy)biphenyl-4-yl 4-(heptyloxy)benzoate (5b). Yield: 71%. ¹H NMR δ [ppm]: 8.10 (d, 2H, $J = 8.8$ Hz, Ar-H), 7.51 (d, 2H, $J = 8.8$ Hz, Ar-H), 7.44 (d, 2H, $J = 8.8$ Hz, Ar-H), 7.17 (d, 2H, $J = 8.4$ Hz, Ar-H), 6.90 (overlapped, dd, 4H, $J = 8.8$ Hz, Ar-H), 5.81 (m, 1H, HC=CH₂), 4.95 (m, 2H, HC=CH₂), 3.98 (t, 2H, $J = 6.4$, 6.8 Hz, OCH₂), 4.02 (t, 2H, $J = 6.4$, 6.8 Hz, OCH₂), 2.03 (m, 2H, CH₂HC=CH₂), 1.81 (m, 4H, OCH₂CH₂), 1.50 (m, 4H, OCH₂CH₂CH₂), 1.31–1.19 (m, 16H, (CH₂)₈), 0.90 (t, 3H, $J = 6.6$ Hz, CH₃). ¹³C NMR δ [ppm]: 165.36, 163.93, 159.16, 150.43, 139.54, 138.91, 133.23, 132.63, 128.44, 128.00, 122.31, 122.03, 115.23, 114.70, 114.46, 68.72, 68.51, 34.14, 32.11, 29.86, 29.77, 29.73, 29.67, 29.48, 29.46, 29.37, 29.29, 26.41, 26.31, 22.94, 14.39. EI-MS (m/z): Found: 556.4. Calc. 556.7. Anal. Calc for C₃₇H₄₈O₄: C 79.82%, H 8.69%, found: C 79.58%, H 8.48%

4'-(Undec-10-enyloxy)biphenyl-4-yl 4-(octyloxy)benzoate (5c). Yield: 66%. ¹H NMR δ [ppm]: 8.08 (d, 2H, $J = 8.4$ Hz, Ar-H), 7.51 (d, 2H, $J = 8.4$ Hz, Ar-H), 7.43 (d, 2H, $J = 8.4$ Hz, Ar-H), 6.90 (overlapped, dd, 4H, $J = 8.8$ Hz, Ar-H), 5.74 (m, 1H, HC=CH₂), 4.89 (m, 2H, HC=CH₂), 3.98 (t, 2H, $J = 6.4$ Hz, OCH₂), 3.93 (t, 2H, $J = 6.4$ Hz, OCH₂), 1.98 (m, 2H, CH₂HC=CH₂), 1.74 (m, 4H, OCH₂CH₂), 1.46–1.35 (m, 4H, OCH₂CH₂CH₂), 1.34–1.16 (m, 18H, (CH₂)₉), 0.83 (t, 3H, $J = 6.8$ Hz, CH₃). ¹³C NMR δ [ppm]: 165.36, 163.93, 159.16, 150.43, 139.54, 138.91, 133.22, 132.63, 128.44, 128.01, 122.32, 122.03, 115.23, 114.69, 114.46, 68.72, 68.51, 34.13, 32.15, 29.86, 29.77, 29.73, 29.67, 29.55, 29.47, 29.46, 29.29, 26.41, 26.345, 22.99, 14.40. EI-MS (m/z): Found: 570.5. Calc: 570.8. Anal. Calc for C₃₈H₅₀O₄: C 79.96%, H 8.83%, found: C 79.63%, H 8.59%

4'-(Undec-10-enyloxy)biphenyl-4-yl 4-(dodecyloxy)benzoate (5d). Yield: 56%. ¹H NMR δ [ppm]: 8.15 (d, 2H, $J = 8.8$ Hz, Ar-H), 7.57 (d, 2H, $J = 8.4$ Hz, Ar-H), 7.50 (d, 2H, $J = 8.4$ Hz, Ar-H), 7.23 (d, 2H, $J = 8.8$ Hz, Ar-H), 6.97 (overlapped, dd, 4H, $J = 8.8$ Hz, Ar-H), 5.81 (m, 1H, HC=CH₂), 4.98 (m, 2H, HC=CH₂), 4.04 (t, 2H, $J = 6.4$ Hz, OCH₂), 3.99 (t, 2H, $J = 6.4$ Hz, OCH₂), 2.06 (m, 2H, CH₂HC=CH₂), 1.81 (m, 4H, OCH₂CH₂), 1.44 (m, 4H, OCH₂CH₂CH₂), 1.38–1.27 (m, 26H, (CH₂)₁₃), 0.89 (t, 3H, $J = 6.4$ Hz, CH₃). ¹³C NMR δ [ppm]: 165.37, 163.94, 159.16, 150.43, 139.55, 138.92, 133.23, 132.64, 128.45, 128.02, 122.03, 121.55, 115.23, 114.70, 114.47, 68.73, 68.52, 34.14, 32.27, 30.01, 29.98, 29.94, 29.91, 29.87, 29.78, 29.74, 29.72, 29.69, 29.67, 29.47, 29.30, 26.42, 26.35, 23.03, 14.44. EI-MS (m/z): Found: 626.5. Calc.:626.9. Anal. Calc for C₄₂H₅₈O₄: 80.47%, H 9.33%, found: C 80.30%, H 9.04%

4'-(Undec-10-enyloxy)biphenyl-4-yl 3,5-di(hexyloxy)benzoate (5e). Yield: 78%. ¹H NMR δ [ppm]: 7.60 (d, 2H, $J = 8.5$ Hz, Ar-H), 7.53 (d, 2H, $J = 10.1$ Hz, Ar-H), 7.37 (s, 2H, Ar-H), 7.27 (d, 2H, $J = 8.6$ Hz, Ar-H), 6.99 (d, 2H, $J = 8.7$ Hz, Ar-H), 6.75 (s, 1H, Ar-H), 5.84 (m, 1H, HC=CH₂), 4.98 (m, 2H, HC=CH₂), 4.02 (m, 6H, OCH₂), 2.08 (m, 2H, CH₂HC=CH₂), 1.82 (m, 6H, OCH₂CH₂), 1.49–1.20 (m, 24H, (CH₂)₁₂), 0.97 (t, 6H, $J = 6.8$ Hz, CH₃). ¹³C NMR (CDCl₃) δ [ppm]: 165.59, 160.71, 159.20, 150.29, 139.64, 139.13, 133.14, 131.62, 128.51, 128.12, 122.27, 115.23, 114.53, 108.62, 107.55, 38.83, 68.52, 34.21, 31.96, 31.92, 29.79, 29.70, 29.55, 29.34, 26.46, 26.10, 23.00, 14.43. EI-MS (m/z): Found, 642.6; Calc. 642.4

4'-(Undec-10-enyloxy)biphenyl-4-yl 3,5-di(dodecyloxy)benzoate (5f). Yield: 60%. ¹H NMR δ [ppm]: 7.58 (d, 2H, $J = 8.6$ Hz, Ar-H), 7.51 (d, 2H, $J = 8.6$ Hz, Ar-H), 7.33 (s, 2H, Ar-H), 7.24 (d, 2H, $J = 8.8$ Hz, Ar-H), 6.97 (d, 2H, $J = 8.7$ Hz, Ar-H), 6.71 (s, 1H, Ar-H), 5.84 (m, 1H, HC=CH₂), 4.98 (m, 2H, HC=CH₂), 4.00 (m, 6H, OCH₂), 2.05 (m, 2H, CH₂HC=CH₂), 1.80 (m, 6H, OCH₂CH₂), 1.49–1.20 (m, 54H, (CH₂)₁₂), 0.88 (t, 6H, $J = 6.5$ Hz, CH₃). ¹³C NMR (CDCl₃) δ [ppm]: 165.51, 160.75, 159.24, 150.36, 139.57, 139.12, 133.19, 131.69, 128.47, 128.07, 122.22, 115.29, 114.47, 108.70, 107.64, 68.87, 68.56, 34.15, 32.28, 30.00, 29.95, 29.88, 29.74, 29.70, 29.58, 29.48, 29.32, 26.40, 23.03, 14.43. EI-MS (m/z): Found, 810.9; Calc. 810.6

4'-(Undec-10-enyloxy)biphenyl-4-yl 3,4,5-tris(butyloxy)benzoate (5g). Yield: 76%. ¹H NMR δ [ppm]: 7.59 (d, 2H, $J = 8.4$ Hz, Ar-H), 7.51 (d, 2H, $J = 8.8$ Hz, Ar-H), 7.43 (s, 2H, Ar-H), 7.23 (d, 2H, $J = 8.4$ Hz, Ar-H), 6.97 (d, 2H, $J = 8.8$ Hz, Ar-H),

5.84 (m, 1H, HC=CH₂), 4.98 (m, 2H, HC=CH₂), 4.07 (m, 6H, OCH₂), 4.00 (t, 2H, *J* = 6.8 Hz, 2.05 (m, 2H, CH₂HC=CH₂), 1.84–1.73 (m, 8H, OCH₂CH₂), 1.60–1.20 (m, 20H, (CH₂)₅), 1.00 (t, 9H, *J* = 6.5 Hz, CH₃). ¹³C NMR (CDCl₃) δ [ppm]: 165.46, 159.23, 153.41, 150.41, 143.64, 139.56, 139.18, 133.18, 128.46, 128.06, 124.39, 122.30, 115.28, 114.47, 109.20, 73.60, 69.45, 68.55, 34.15, 32.74, 31.76, 29.87, 29.78, 29.74, 29.69, 29.48, 29.31, 26.43, 19.63, 19.52, 14.16. EI-MS (*m/z*): Found, 658.6; Calc. 658.4

4'-(Undec-10-enyloxy)biphenyl-4-yl 3,4,5-tris(dodecyloxy)benzoate (5h). Yield: 42%. ¹H NMR (400 MHz, CDCl₃) δ [ppm]: 7.59 (d, 2H, *J* = 8.8 Hz, Ar-H), 7.52 (d, 2H, *J* = 8.8 Hz, Ar-H), 7.43 (s, 2H, Ar-H), 7.23 (d, 2H, *J* = 8.4 Hz, Ar-H), 6.98 (d, 2H, *J* = 8.8 Hz, Ar-H), 5.81 (m, 1H, HC=CH₂), 4.95 (m, 2H, HC=CH₂), 4.04 (m, 8H, OCH₂), 2.04 (m, 2H, CH₂HC=CH₂), 1.82 (m, 8H, OCH₂CH₂), 1.49 (m, 8H, OCH₂CH₂CH₂), 1.38–1.27 (m, 58H, (CH₂)₂₉), 0.88 (m, 9H, CH₃). ¹³C NMR (CDCl₃) δ [ppm]: 165.44, 159.20, 153.36, 150.38, 143.56, 139.52, 139.03, 133.14, 128.43, 128.02, 124.34, 122.28, 115.24, 114.46, 109.14, 73.95, 69.72, 68.51, 34.13, 32.29, 32.27, 30.72, 30.10, 30.08, 30.07, 30.04, 30.00, 29.98, 29.92, 29.86, 29.77, 29.75, 29.73, 29.70, 29.66, 29.46, 29.29, 26.45, 26.43, 26.41, 23.04, 23.03, 14.42. EI-MS (*m/z*): Found: 995.0. Calc. 995.5. Anal. Calc for C₆₆H₁₀₈O₄: 79.63%, H 10.93%, found: C 79.49%, H 10.24%.

Octakis[(11-(4'-(1-(4-alkoxybenzoyloxy)biphenyl-4-yloxy)undecyl)dimethylsiloxy)]silsesquioxane (7a–h)

General synthetic procedures of 7a–h. 4'-Hydroxybiphenyl undecene-1-yloxy-4-n-pentylbenzoate (50.0 mg, 0.095 mmol) was dissolved in 3 mL of dry toluene followed by octakis (hydrodimethylsiloxy)octasilsesquioxane (POSS) (11.2 mg, 0.011 mmol). The reaction mixture was purged with nitrogen gas for 30 min before Pt(dvs) (10.2 μL) was added. The reaction was stirred at 42 °C under nitrogen for 12 h. After that, toluene was removed under reduced pressure. The crude product was repeatedly column chromatographed on silica gel using dichloromethane–hexane (V : V = 1 : 1) and then dichloromethane and ethyl acetate (V : V = 95 : 5) as eluent to afford pure 7a–h. The relatively low yields for some of POSS molecules are because of repeated column chromatography.

Octakis[(11-(4'-(1-(4-pentyloxybenzoyloxy)biphenyl-4-yloxy)undecyl)dimethylsiloxy)]silsesquioxane (7a)

Yield: 15%. ¹H NMR δ [ppm]: 8.15 (d, 16H, *J* = 8.8 Hz, Ar-H), 7.55 (d, 16H, *J* = 8.4 Hz, Ar-H), 7.48 (d, 16H, *J* = 8.4 Hz, Ar-H), 7.26 (d, overlapped with CDCl₃, 16H, Ar-H), 6.97 (overlapped dd, 32H, Ar-H), 4.11 (t, 16H, *J* = 6.4 Hz, OCH₂), 4.02 (t, 16H, *J* = 6.4 Hz, OCH₂), 1.81 (m, 32H, OCH₂CH₂), 1.46 (m, 32H, OCH₂CH₂CH₂), 1.38–1.23 (m, 128H, (CH₂)₈), 0.95 (t, 24H, *J* = 7.05, CH₃), 0.60 (m, 16H, SiCH₂), 0.13 (s, 48H, Si(CH₃)₂). ¹³C NMR δ [ppm]: 165.37, 163.91, 159.15, 150.40, 138.90, 133.18, 132.64, 128.44, 128.01, 122.33, 122.02, 115.20, 114.67, 68.70, 68.52, 33.89, 32.29, 30.05, 30.02, 29.72, 29.17, 28.51, 26.05, 23.35,

23.05, 22.79, 18.07, 14.45, 14.34, 0.34. ²⁹Si NMR δ [ppm]: 12.33, –108.65.

Octakis[(11-(4'-(1-(4-heptyloxybenzoyloxy)biphenyl-4-yloxy)undecyl)dimethylsiloxy)]silsesquioxane (7b)

Yield: 56%. ¹H NMR δ [ppm]: 8.14 (d, 16H, *J* = 8.8 Hz, Ar-H), 7.55 (d, 16H, *J* = 8.4 Hz, Ar-H), 7.48 (d, 16H, *J* = 8.8 Hz, Ar-H), 7.22 (overlapped with CDCl₃, 16H, Ar-H), 6.97 (overlapped dd, 32H, Ar-H), 4.03 (t, 16H, *J* = 0.66 Hz, OCH₂), 3.96 (t, 16H, *J* = 6.6 Hz, OCH), 1.79 (m, 32H, OCH₂CH₂), 1.46 (m, 32H, OCH₂CH₂CH₂), 1.32–1.19 (m, 160H, (CH₂)₁₀), 0.92 (t, 24H, *J* = 6.8 Hz, CH₃), 0.60 (m, 16H, SiCH₂), 0.13 (s, 48H, Si(CH₃)₂). ¹³C NMR δ [ppm]: 165.35, 163.92, 159.18, 150.41, 138.89, 133.18, 132.64, 128.43, 127.99, 122.32, 122.05, 115.21, 114.69, 68.72, 68.53, 33.87, 32.12, 30.13, 30.11, 30.06, 29.92, 29.84, 29.77, 29.50, 29.39, 26.52, 26.32, 23.39, 22.95, 18.13, 14.40, 0.34. ²⁹Si NMR δ [ppm]: 12.93, –108.60.

Octakis[(11-(4'-(1-(4-octyloxybenzoyloxy)biphenyl-4-yloxy)undecyl)dimethylsiloxy)]silsesquioxane (7c)

Yield: 27%. ¹H NMR δ [ppm]: 8.14 (d, 16H, *J* = 8.4 Hz, Ar-H), 7.55 (d, 16H, *J* = 8.4 Hz, Ar-H), 7.48 (d, 16H, *J* = 8.4 Hz, Ar-H), 7.22 (d, 16H, *J* = 8.4 Hz, Ar-H), 6.97 (overlapped dd, 32H, Ar-H), 4.03 (t, 16H, *J* = 6.4 Hz, OCH₂), 3.97 (t, 16H, *J* = 6.4 Hz, OCH₂), 1.80 (m, 32H, OCH₂CH₂), 1.48 (m, 32H, OCH₂CH₂CH₂), 1.32–1.26 (m, 176H, (CH₂)₁₁), 0.88 (t, 24H, *J* = 6.8 Hz, CH₃), 0.60 (m, 16H, SiCH₂), 0.13 (s, 48H, Si(CH₃)₂). ¹³C NMR δ [ppm]: 165.35, 163.92, 159.17, 150.41, 138.89, 133.17, 132.64, 128.43, 127.99, 122.32, 122.04, 115.20, 114.69, 68.72, 68.52, 33.87, 32.16, 30.13, 30.11, 30.06, 29.91, 29.84, 29.80, 29.76, 29.69, 29.57, 29.49, 26.52, 26.36, 23.39, 23.00, 18.12, 14.42, 0.34. ²⁹Si NMR δ [ppm]: 12.70, –108.68.

Octakis[(11-(4'-(1-(4-dodecyloxybenzoyloxy)biphenyl-4-yloxy)undecyl)dimethylsiloxy)]silsesquioxane (7d)

Yield: 56%. ¹H NMR δ [ppm]: 8.14 (d, 16H, *J* = 8.4 Hz, Ar-H), 7.55 (d, 16H, *J* = 8.4 Hz, Ar-H), 7.48 (d, 16H, *J* = 8.8 Hz, Ar-H), 7.22 (d, 16H, *J* = 7.2 Hz, Ar-H), 6.93 (overlapped dd, 32H, Ar-H), 4.03 (t, 16H, *J* = 6.8 Hz, OCH₂), 3.96 (t, 16H, *J* = 6.4 Hz, OCH₂), 1.79 (m, 32H, OCH₂CH₂), 1.48 (m, 32H, OCH₂CH₂CH₂), 1.38–1.27 (m, 240H, (CH₂)₁₅), 0.88 (t, 24H, *J* = 6.8 Hz, CH₃), 0.60 (m, 16H, SiCH₂), 0.13 (s, 48H, Si(CH₃)₂). ¹³C NMR δ [ppm]: 165.34, 163.93, 159.18, 150.42, 138.89, 133.18, 132.64, 128.43, 127.99, 122.32, 122.05, 115.21, 114.69, 68.73, 68.53, 33.84, 32.28, 30.13, 30.11, 30.08, 30.06, 30.01, 29.99, 29.94, 29.91, 29.83, 29.76, 29.73, 29.70, 29.49, 26.51, 26.35, 23.38, 23.03, 18.12, 14.44, 0.33. ²⁹Si NMR δ [ppm]: 12.75, –108.68.

Octakis[(11-(4'-(1-(3,5-dihexyloxybenzoyloxy)biphenyl-4-yloxy)undecyl)dimethylsiloxy)]silsesquioxane (7e)

Yield: 73%. ¹H NMR δ [ppm]: 7.56 (d, 16H, *J* = 8.4 Hz, Ar-H), 7.48 (d, 16H, *J* = 8.4 Hz, Ar-H), 7.31 (s, 16H, Ar-H), 7.22(d, 16H, *J* = 8.4 Hz, Ar-H), 6.95 (d, 16H, *J* = 8.8 Hz, Ar-H), 6.70 (s, 8H, Ar-H), 3.98 (m, 48H, OCH₂), 1.80 (m, 48H, OCH₂CH₂), 1.60–1.20 (m, 224H, (CH₂)₁₄), 0.62 (m, 16H, Si-CH₂), 0.14 (s, 48H, Si-CH₃). ¹³C NMR (CDCl₃) δ [ppm]: 165.56, 160.70,

159.20, 150.27, 139.09, 133.09, 131.61, 128.48, 128.08, 122.27, 115.19, 108.60, 107.52, 68.82, 68.52, 33.94, 31.96, 30.17, 30.12, 29.96, 29.90, 29.79, 29.55, 26.56, 26.10, 23.43, 23.00, 18.15, 14.43, 0.11. ^{29}Si NMR (CDCl_3) δ [ppm]: 12.78, -108.71

Octakis[(11-(4'-(1-(3,5-didodecyloxybenzoyloxy)biphenyl-4-oxyl)undecyl)dimethylsiloxy)silsesquioxane (7f)

Yield: 25%. ^1H NMR δ [ppm]: 7.57 (d, 16H, $J = 8.4$ Hz, Ar-H), 7.49 (d, 16H, $J = 8.4$ Hz, Ar-H), 7.32 (s, 16H, Ar-H), 7.23 (d, 16H, $J = 8.4$ Hz, Ar-H), 6.95 (d, 16H, $J = 8.8$ Hz, Ar-H), 6.71 (s, 8H, Ar-H), 4.00 (m, 48H, $J = 6.4$ Hz, OCH_2), 1.80 (m, 16H, OCH_2CH_2), 1.60–1.20 (m, 464H, $(\text{CH}_2)_{26}$), 0.89 (t, 48H, $J = 6.4$ Hz, CH_3), 0.62 (m, 16H, Si- CH_2), 0.15 (s, 48H, Si- CH_3). ^{13}C NMR (CDCl_3) δ [ppm]: 165.49, 160.75, 159.24, 150.35, 139.10, 133.16, 131.69, 128.45, 128.04, 122.22, 115.26, 108.70, 107.62, 68.86, 68.58, 33.83, 32.29, 30.00, 29.96, 29.75, 29.59, 29.52, 26.52, 26.41, 23.37, 23.04, 18.11, 14.43, 0.07. ^{29}Si NMR (CDCl_3) δ [ppm]: 12.75, -108.65.

Octakis[(11-(4'-(1-(3,4,5-tributyloxybenzoyloxy)biphenyl-4-oxyl)undecyl)dimethylsiloxy)silsesquioxane (7g)

Yield: 57%. ^1H NMR δ [ppm]: 7.58 (d, 16H, $J = 8.4$ Hz, Ar-H), 7.49 (d, 16H, $J = 8.4$ Hz, Ar-H), 7.42 (s, 16H, Ar-H), 7.22 (d, 16H, $J = 8.4$ Hz, Ar-H), 6.95 (d, 16H, $J = 8.8$ Hz, Ar-H), 4.06–3.9 (m, 48H, OCH_2), 1.80 (m, 64H, OCH_2CH_2), 1.60–1.20 (m, 224H, $(\text{CH}_2)_{14}$), 0.98 (m, 72H, CH_3), 0.60 (m, 16H, Si- CH_2), 0.14 (s, 48H, Si- CH_3). ^{13}C NMR (CDCl_3) δ [ppm]: 165.43, 159.25, 153.41, 150.43, 143.67, 139.04, 133.16, 131.20, 129.19, 128.44, 128.03, 124.40, 122.30, 115.26, 109.24, 73.60, 72.16, 69.47, 68.58, 33.87, 32.75, 31.77, 30.82, 30.12, 29.85, 29.33, 26.54, 23.40, 19.63, 19.52, 18.15, 14.35, 14.15, 0.09. ^{29}Si NMR (CDCl_3) δ [ppm]: 13.03, -108.51

Octakis[(11-(4'-(1-(3,4,5-tridodecyloxybenzoyloxy)biphenyl-4-oxyl)undecyl)dimethylsiloxy)silsesquioxane (7h)

Yield: 45%. ^1H NMR δ [ppm]: 7.56 (d, 16H, $J = 8.4$ Hz, Ar-H), 7.48 (d, 16H, $J = 8.8$ Hz, Ar-H), 7.41 (s, 16H, Ar-H), 7.22 (d, 16H, $J = 8.4$ Hz, Ar-H), 6.94 (d, 16H, $J = 8.8$ Hz, Ar-H), 4.03 (m, 64H, OCH_2), 1.81 (m, 64H, OCH_2CH_2), 1.52–1.41 (m, 64H, $\text{OCH}_2\text{CH}_2\text{CH}_2$), 1.41–1.16 (m, 496H, $(\text{CH}_2)_{31}$), 0.88 (m, 72H, CH_3), 0.61 (m, 16H, Si- CH_2), 0.13 (s, 48H, Si- $(\text{CH}_3)_2$). ^{13}C NMR δ [ppm]: 153.37, 128.44, 128.02, 122.30, 115.22, 109.13, 69.74, 33.88, 32.30, 32.28, 30.74, 30.11, 30.10, 30.05, 30.01, 29.99, 29.94, 29.76, 29.74, 29.71, 26.46, 23.39, 23.04, 23.03, 18.12, 14.43, 0.34. ^{29}Si NMR (CDCl_3) δ [ppm]: 13.08, -108.59

Acknowledgements

This work was funded by the Institute of Materials Research and Engineering (IMRE), A*STAR (Agency for Science, Technology and Research), Singapore.

References and notes

1 P. D. Lickiss and F. Rataboul, Fully Condensed Polyhedral Oligosilsesquioxanes (POSS): From Synthesis to Application, in: A. F. Hilland and M. J. Fink, *Advances in Organometallic*

- Chemistry*, vol. 57, ed. R. West, The Netherlands, Elsevier Inc., 2008, pp. 1–116.
- 2 D. B. Cordes, P. D. Lickiss and F. Rataboul, *Chem. Rev.*, 2010, **110**, 2081–2173.
 - 3 R. Y. Kannan, H. J. Salacinski, P. E. Butler and A. M. Seifalian, *Acc. Chem. Res.*, 2005, **38**, 879–884.
 - 4 H. Liu, S. Zheng and K. Nie, *Macromolecules*, 2005, **38**, 5088–5097.
 - 5 J. Miao, L. Cui, H. P. Lau, P. T. Mather and L. Zhu, *Macromolecules*, 2007, **40**, 5460–5470.
 - 6 L. Zhang, Q. Yang, H. Yang, J. Liu, H. Xin, B. Mezari, P. C. M. M. Magusin, H. C. L. Abbenhuis, R. A. van Santen and C. Li, *J. Mater. Chem.*, 2008, **18**, 450–457.
 - 7 K. Y. Mya, Y. Wang, I. L. Shen, J. Xu, Y. Wu, X. Lu and C. He, *J. Polym. Sci., Part A: Polym. Chem.*, 2009, **47**, 4602–4616.
 - 8 J. Xu, X. Li, C. M. Cho, C. L. Toh, L. Shen, K. Y. Mya, X. Lu and C. He, *J. Mater. Chem.*, 2009, **19**, 4740–4745.
 - 9 J. Huang, C. He, X. Liu, J. Xu, C. S. S. Tay and S. Y. Chow, *Polymer*, 2005, **46**, 7018–7027.
 - 10 S. S. Nobre, C. D. S. Brites, R. A. S. Ferreira, V. Z. Bermudez, C. Carcel, J. J. E. Moreau, J. Rocha, M. C. M. Wong and L. D. Carlos, *J. Mater. Chem.*, 2008, **18**, 4172–4182.
 - 11 A. Strachota, P. Whelan, J. Kriz, J. Brus, M. Urbanova, M. Slouf and L. Matejka, *Polymer*, 2007, **48**, 3041–3058.
 - 12 M. J. Abad, L. Barral, D. P. Fasce and R. J. J. Williams, *Macromolecules*, 2003, **36**, 3128–3135.
 - 13 I. A. Zucchi, M. J. Galante, R. J. J. Williams, E. Franchini, J. Galy and J. F. Gerard, *Macromolecules*, 2007, **40**, 1274–1282.
 - 14 E. A. Drylie, C. D. Andrews, M. A. Hearshaw, C. Jimenez-Rodriguez, A. Slawin, D. J. Cole-Hamilton and R. E. Morris, *Polyhedron*, 2006, **25**, 853–858.
 - 15 L. Cui, J. P. Collet, G. Xu and L. Zhu, *Chem. Mater.*, 2006, **18**, 3503–3512.
 - 16 F.-H. Kreuzer, R. Maurer and P. Spes, *Makromol. Chem. Macromol. Symp.*, 1991, **50**, 215–228.
 - 17 I. M. Saez and P. Styring, *Adv. Mater.*, 1996, **8**, 1001–1005.
 - 18 R. M. Laine, C. Zhang, A. Sellinger and L. Viculis, *Appl. Organomet. Chem.*, 1998, **12**, 715–723.
 - 19 C. X. Zhang, T. J. Bunning and R. M. Laine, *Chem. Mater.*, 2001, **13**, 3653–3662.
 - 20 M. C. Gravel, C. Zhang, M. Dinderman and R. M. Laine, *Appl. Organomet. Chem.*, 1999, **13**, 329–336.
 - 21 I. M. Saez and J. W. Goodby, *Liq. Cryst.*, 1999, **26**, 1101–1105.
 - 22 R. Elsäßer, G. H. Mehl, J. W. Goodby and D. J. Photinos, *Chem. Commun.*, 2000, 851–852.
 - 23 M. O'Neill and S. M. Kelly, *Adv. Mater.*, 2003, **15**, 1135–1146.
 - 24 I. M. Saez, J. W. Goodby and R. M. Richardson, *Chem.–Eur. J.*, 2001, **7**, 2758–2764.
 - 25 I. M. Saez and J. W. Goodby, *J. Mater. Chem.*, 2001, **11**, 2845–2851.
 - 26 C. X. Zhang and R. M. Laine, *J. Am. Chem. Soc.*, 2000, **122**, 6979–6988.
 - 27 C. Keith, G. Dantlgraber, R. A. Reddy, U. Baumeister, M. Prehm, H. Hahn, H. Lang and C. Tschierske, *J. Mater. Chem.*, 2007, **17**, 3796–3805.
 - 28 J. Miao and L. Zhu, *J. Phys. Chem. B*, 2010, **114**, 1897–1887.
 - 29 C. Ornelas, D. Mery, E. Cloutet, J. R. Aranzas and D. Astruc, *J. Am. Chem. Soc.*, 2008, **130**, 1495–1506.
 - 30 G. H. Mehl and I. M. Saez, *Appl. Organomet. Chem.*, 1999, **13**, 261–272.
 - 31 Q. Pan, X. Chen, X. Fan, Z. Shen and Q. Zhou, *J. Mater. Chem.*, 2008, **18**, 3481–3488.
 - 32 K. D. Gresham, C. M. McHugh, T. J. Bunning, R. L. Crane, H. E. Klei and E. T. Samulski, *J. Polym. Sci., Part A: Polym. Chem.*, 1994, **32**, 2039–47.
 - 33 J. Xu, T. C. Ling and C. He, *J. Polym. Sci., Part A: Polym. Chem.*, 2008, **46**, 4691–4703.
 - 34 H. C. Holst, T. Pakula and H. Meier, *Tetrahedron*, 2004, **60**, 6765–6775.
 - 35 J. Barbera, M. Bardaji, J. Jimenez, A. Laguna, M. P. Martinez, L. Oriol, J. L. Serrano and I. Zaragoza, *J. Am. Chem. Soc.*, 2005, **127**, 8994–9002.
 - 36 G. H. Mehl and J. W. Goodby, *Angew. Chem., Int. Ed. Engl.*, 1996, **35**, 2641–2643.
 - 37 G. H. Mehl, A. J. Thornton and J. W. Goodby, *Mol. Cryst. Liq. Cryst.*, 1999, **332**, 455–461.
 - 38 M. F. Achard, S. Lecommandoux and F. Hardouin, *Liq. Cryst.*, 1995, **19**, 581–587.